Controls of the Foreland-Deformation Pattern in the Orogen-Foreland Shortening System: Constraints from High-Resolution Geodynamic Models

Sibiao Liu[1, 2, 3], Stephan V. Sobolev[1, 2], Andrey Y. Babeyko[1], Michael Pons[2, 3]

[1]GEOMAR Helmholtz Centre for Ocean Research Kiel, Kiel, Germany

[2]German Research Center for Geosciences GFZ, Potsdam, Germany

[3]Institute of Earth and Environmental Science, University of Potsdam, Potsdam, Germany

Corresponding author: S. Liu (sliu@geomar.de)

Key Points:

- Thicknesses of the orogenic crust and the foreland lithosphere control the foreland shortening mode (pure-shear or simple-shear).
- Foreland weak sediments and the upper lithosphere of the weaker orogen control the foreland tectonic style (thin-skinned or thick-skinned).
- High-resolution numerical models successfully reproduce foreland-deformation patterns in several natural orogen-foreland systems.

Abstract

Controls on the deformation pattern (shortening mode and tectonic style) of orogenic forelands during tectonic shortening remain poorly understood. Here, we use high-resolution 2D thermomechanical models to demonstrate that the orogenic crustal thickness and the foreland lithospheric thickness control the shortening mode in the foreland. Pure-shear shortening occurs when the orogenic crust is not thicker than the foreland crust or when it is thick but the foreland lithosphere is thin (< 70-80 km, as in the Puna foreland case). Simple-shear shortening, characterized by foreland underthrusting beneath the orogen, arises when the orogenic crust is much thicker than the foreland crust. The thickened orogenic crust causes the orogen to have high gravitational potential energy that prevents deformation in the orogen and forces shortening in the foreland, while the weak orogenic lithosphere allows the foreland lithosphere to underthrust beneath the orogen. Our models present fully thick-skinned, fully thin-skinned, and intermediate tectonics styles. The first tectonics forms in a pure-shear shortening mode whereas the others require a simple-shear mode and the presence of thick (> ~4 km) sediments that are mechanically weak (friction coefficient < ~0.05) or are weakened rapidly during the deformation. Fully thin-skinned tectonics in the foreland, as in the Subandean Ranges, forms in thick and weak sediments and requires the strength of the orogenic upper lithosphere to be less than one-third of that of the foreland upper lithosphere. Our models successfully reproduce foreland-deformation patterns in the Central and Southern Andes and the Laramide province.

1 Introduction

In the orogen-foreland shortening system, pure-shear and simple-shear are two common shortening modes in foreland deformation belts. Pure-shear shortening is characterized by a vertically quasi-homogeneous thickening of the foreland crust, while the foreland lithosphere underthrusts beneath the orogen along a low-angle detachment fault in the simple-shear mode. During shortening, the crustal-scale deformation in the foreland forms either shallow thin-skinned or deeper thick-skinned tectonics (e.g., Lacombe & Bellahsen, 2016; Pfiffner, 2017). In the former, the shortened rocks overlie an almost undeformed basement along a shallow basal décollement fault, while the basement is deformed above a deep crustal detachment zone in the latter (Dahlen, 1990). Previous regional studies have observed these different foreland-deformation patterns (i.e., shortening modes and tectonic styles) in natural orogen-foreland systems, for example in the Central-Southern Andes (e.g., Ramos et al., 2004; Giambiagi et al., 2011; Mescua et al., 2016), Southern Canadian Rockies (e.g., Price, 1981; Stockmal et al., 2007), Laramide Rocky Mountains (e.g., DeCelles, 2004; Yonkee & Weil, 2015), Taiwan and Alps (e.g., Lacombe & Mouthereau, 2002; Mouthereau & Lacombe, 2006; Bellahsen et al., 2014; Lacombe & Bellahsen, 2016; Pfiffner, 2016), and the Zagros (e.g., Mouthereau et al., 2006, 2007; Jammes & Huismans, 2012; Mouthereau et al., 2012; Nilfouroushan et al., 2013).

Transition between the two shortening modes and the way thin-skinned and thick-skinned tectonics interact are unclear. Previous studies have attempted to quantify some of the relationships between shallow and deep lithospheric structures and processes; these studies suggested that the foreland-deformation pattern is related to the contrast of lithospheric strength between the orogen and its foreland (e.g., Babeyko et al., 2006; Jammes & Huismans, 2012; Mouthereau et al., 2013; Erdős et al., 2015). For instance, Jammes and Huismans (2012) demonstrated that systems with a weak orogen show the deformation of mountain building accommodated on a few thick-skinned crustal-scale thrusts with moderate displacement and by distributed crustal thickening, as observed in the Zagros. This weak crust may be the result of its mechanically weak composition (i.e., low viscosity) or high geothermal gradient (Nilfouroushan et al., 2013). Mouthereau et al. (2013) found a relationship between the orogenic deformation and the foreland lithospheric strength through the dependence on the age of the lithosphere during shortening. A thin-skinned thrust zone would form in the orogen if its foreland is old, cold, and strong. Erdős et al. (2015) supported that synorogenic sedimentation on the external parts of an orogen may provide a first-order control on its style of basement deformation. In sediment-starved orogens, such as the Southern Urals case (Brown et al., 1997), the thick-skinned deformation is mainly located in the orogenic core, whereas in sediment-loaded orogens, such as the Swiss Alps (Mosar, 1999), this basement-involved structure appears in both the axial zone and the foreland. Babeyko et al. (2006) demonstrated that a sudden drop of the mechanical strength of foreland sediments east of the Altiplano Plateau is responsible for the shift of the shortening mode from pure-shear to simple-shear, as well as for the formation of the Subandean foreland deformation zones.

However, these studies mainly focused on structural styles of the orogen and foreland crustal-scale deformation has received less attention. In particular, the exact nature of variations in the lithospheric strength and sediment weakening affecting the evolution of foreland deformation is still not well understood. In addition, the question of whether controlled factors from these studies can be applied to explain the deformation patterns in other forelands remains open. The above-cited models also did not explore more details of the foreland-deformation features (e.g., the fault direction) due to the lack of necessary numerical resolution at that time. Recent progress in numerical modeling techniques allows for an extension of this research to higher-resolution lithospheric models, which is the subject of the current study.

The long-term strength of continental lithosphere is primarily controlled by its composition and temperature, which strongly depend on depth, i.e., the lithospheric thickness and the crustal thickness (e.g., Kusznir & Park, 1986; Ellis, 1988; Cloetingh & Burov, 1996). A thicker lithosphere is colder and stronger due to its smaller temperature gradient. The entire lithospheric strength decreases when the crust is thickened (**Figure A1**). Composition, fluid content (degree of hydration), magmatism, and the thermal/structural inheritance also have some influence on the lithospheric strength (e.g., Kohlstedt et al., 1995; Burov & Watt, 2006; Burov, 2011; Mouthereu et al., 2013; Erdős et al., 2015). For example, the foreland lithosphere in a subduction-dominated orogeny can be weakened by a high degree of hydration or a hot thermal structure due to the subduction process. In this study we address the key (although certainly not all) controlling factors which are thicknesses of thermal lithosphere and of the crust. These two together also automatically determine partition of the lithosphere into the crust and mantle lithosphere, thus also taking into account effect of composition and at least partially.

The sedimentary strength is another critical factor to be taken into account in the development of the foreland-deformation pattern and is related to the friction coefficient of the sediment and its thickness. The mechanically weakened sedimentary layer in the foreland can facilitate the initiation of foreland underthrusting below the orogen during shortening (Babeyko & Sobolev, 2005). This factor should be considered separately from the lithospheric strength. This is because, on the one hand, although the sedimentary layer covering the foreland can be as thick as 8 km or more (Laske et al., 2013), its thickness is still less than 10% of a typical continental lithospheric thickness (~100-200 km thick). Therefore, change of the sediment strength due to thickness change has little effect on the entire lithospheric strength. On the other hand, Byerlee (1978) has also shown that the strength for the first few km of the crust (1-14 km) is determined by the frictional brittle strength (σ_B in Equation 6), which depends highly on pressure rather than compositions. This brittle part has less influence on the strength of the whole lithosphere than the ductile part below. Thus, changes in sedimentary strength due to different compositions hardly affect the brittle strength, much less cause changes in the entire lithospheric strength (**Figure A1**).

Friction coefficient of sediments has a wide range of values from > 0.8 to < 0.05, depending on temperature, composition, pore-fluid pressure, and asperities along the fault surface (Hassani et al., 1997). For example, laboratory experiments indicate that the friction value can be as low as 0.1 if sedimentary rocks contain sufficient clay minerals such as montmorillonite or vermiculite (Byerlee, 1978). Heat-flow data suggest that the value ranges between 0.074 and 0.127 for different subduction zones (Gao & Wang, 2014). Previous geodynamic models constrain this range between 0.5 and 0.015 (Sobolev et al., 2006). A reduction in the friction coefficient can decrease the yield strength of the rock, accelerating its failure. The physical nature of potential frictional weakening in foreland sediments remains controversial. It may be the result of high pore-fluid pressure (lowering the effective confining stress) due to rapid hydrocarbon generation (Cobbold et al., 2004 and reference therein), an increase in precipitation (e.g., Strecker et al., 2007), or compaction under strong compression in the foreland (e.g., Babeyko & Sobolev, 2005). Since we are concerned with the crustal-scale deformation in the foreland, the exact origin of the sedimentary friction drop is not discussed here.

In this study, we first examine how different factors (i.e., lithospheric thickness, crustal thickness, effective friction coefficient of sediments, sedimentary thickness) influence the lithospheric strength of both the orogen and its foreland, and the mechanical strength of foreland sediments. Then we systematically investigate how these parameters control the foreland-deformation pattern during shortening between the orogen and its foreland. Finally, we compare and apply model results to natural orogen-foreland systems such as the Central-Southern Andes and the Laramide province.

2 Numerical Model Description

2.1 Method and Model Geometry

We use the highly scalable parallel code LaMEM (Lithosphere and Mantle Evolution Model; Kaus et al., 2016) to solve three geodynamic conservation equations (see **Appendix A**) to govern material deformation. The initial model contains two structural domains - the orogen and its foreland and is 400 km wide and 400 km deep. As we are interested in the deformation of the foreland crust, we plot our modeling results in the zoom-in area in the top 60 km of the model (dashed grey rectangular in **Figure 1**) with a horizontal distance between 50 km and 330 km. We suppose the effect of side boundary conditions on the modeling result in this area to be minimized (see **Figure S2** in the supporting information, showing that the boundary effects on our zoom-in models can be negligible).

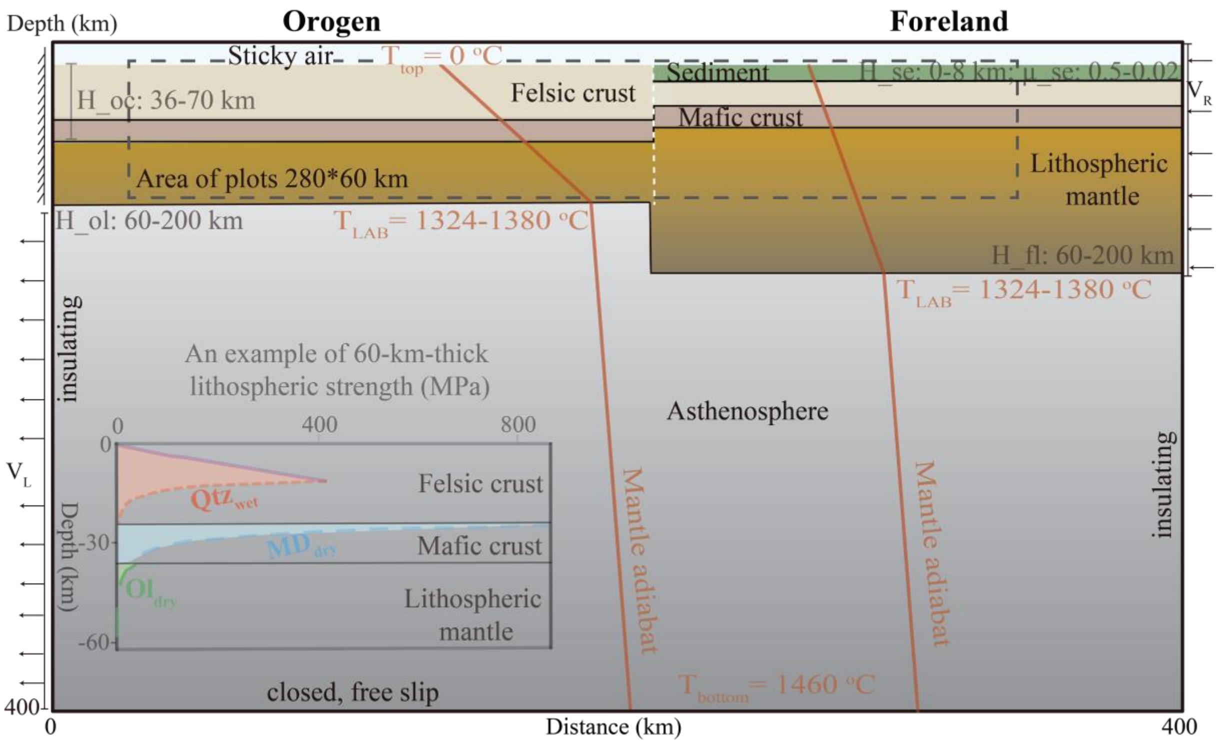

Figure 1. Initial model geometry with thermal-mechanical boundary conditions. Prescribed compressing velocity (V_R) from the right-side boundary is balanced by the uniform outflux velocity (V_L) along the left-side boundary under the orogenic lithosphere. Orange line is the initial thermal field. Temperature of the lithosphere-asthenosphere boundary (T_{LAB}) varies between 1324 °C and 1380 °C, depending on the lithospheric thickness. Crustal thickness in the orogen (H_oc) varies from 36 km to 70 km. Lithospheric thicknesses of the orogen (H_ol) and of the foreland (H_fl) both vary from 60 km to 200 km. Thickness of the foreland sediment (H_se) varies from 0 to 8 km and the value of its friction coefficient (μ_se) is between 0.5 and 0.02. White dashed line is the boundary between the orogen and its foreland. Qtz_{wet}, MD_{dry}, and Ol_{dry} in the example of the 60-km-thick lithospheric strength profile indicate wet quartzite, dry Maryland diabase, and dry olivine, respectively.

Lithospheric thicknesses of the orogen and its foreland in the model vary from 60 km to 200 km. **Figure 1** shows a 60-km-thick lithospheric strength profile, which is an example of a thin and weak orogenic lithosphere due to lithosphere delamination (e.g., Kay & Kay, 1993). The structure of the foreland crust is fixed and contains a 12-km-thick layer of lower mafic crust and a 24-km-thick layer of upper felsic crust with a sedimentary cover of differing thicknesses on the top. By contrast, the thickness of the orogenic crust varies between 36 km and 70 km. A thick orogenic crust could be produced by tectonic shortening during orogenesis in natural orogens such as the Tibetan Plateau and the Central Andes (e.g., Holt & Wallace, 1990; Ramos et al., 2004). Since the range of sedimentary thickness in the foreland is 0-8 km, we apply a 500-m-high grid resolution in the model to ensure that the deformation in such a thin sedimentary layer is being tracked correctly.

2.2 Material Properties and Boundary Conditions

Material properties are taken from the published experimental studies and previous geodynamic models (**Table 1**). All materials contain a fully visco-elasto-plastic rheology, and the ductile deformation mechanisms include diffusion and dislocation creep regimes. The laboratory-derived flow laws of wet quartzite (Qtz_{wet}; Gleason & Tullis, 1995), dry Maryland diabase (MD_{dry}; Mackwell et al., 1998), and wet/dry olivine (Ol_{wet}/Ol_{dry}; Hirth & Kohlstedt, 2003) are used for the felsic crust and its sedimentary cover, the mafic crust, and the lithospheric mantle/asthenosphere, respectively. The felsic crust undergoes frictional-plastic strain softening through a decrease in its friction coefficient from 0.5 to 0.1 over the accumulated strain of 0.5 to 1.5, including the friction angle from 30º to 6º and the cohesion from 20 MPa to 1 MPa (**Table 1**) based on the experience of previous geodynamic models (e.g., Sobolev et al., 2006; Erdős et al., 2015).

Values of thermal parameters are within the range expected for crustal and mantle materials (e.g., Sobolev et al., 2006; Barrionuevo et al., 2021). Radiogenic heat production is 1.0 μW m^{-3} in the felsic crust and 0.3 μW m^{-3} in the mafic crust. The thermal conductivity increases from 2.5 W m^{-1} K^{-1} in the crust to 3.3 W m^{-1} K^{-1} in the mantle to mimic the heat transportation by upper mantle convection without additional model convective motions (e.g., Pysklywec and Beaumont, 2004). Material density is temperature-dependent (**Table 1**). The continental felsic crust has a reference density of 2800 kg m^{-3} at room temperature to reflect that it has a more felsic (silica-rich) composition than the mafic materials below. Density of the sedimentary layer is 300 kg m^{-3} less than the density of the continental felsic rocks at the same temperature. The reference density of the mantle (3300 kg m^{-3}) is consistent with the density of the fertile lithospheric mantle (Poudjom Djomani et al., 2001).

Figure 1 shows the initial thermal-mechanical boundary condition. The initial temperature field increases linearly with depth from the surface (0 °C) to the base of the lithosphere (same temperature as the mantle adiabat at the depth equal to the lithospheric thickness). Increasing the lithospheric thickness leads to a higher temperature at the base of the lithosphere and a smaller thermal gradient inside the lithosphere. As a result, thickening of the lithosphere strengthens the crust and lithospheric mantle. The temperature distribution is adiabatic between the base of the lithosphere and asthenosphere. Temperature at the bottom boundary is 1460 °C, which corresponds to the potential temperature of 1300°C and adiabatic gradient of 0.4 °C/km. The thermal gradient at the side boundaries is taken to be zero which means no horizontal heat flux.

Table 1 *Material properties in the numerical models*

Phase	Sediments; Felsic crust	Mafic crust	Lithospheric mantle	Asthenosphere
Density[1], ρ_0 (kg/m^3)	2500; 2800	3000	3300	3300
Heat expansion, α (K^{-1})	3.7e-5	2.7e-5	3e-5	3e-5
Specific heat, C_p (kJkg^{-1}K^{-1})	1.2	1.2	1.2	1.2
Heat conductivity, k (WK^{-1}m^{-1})	2.5	2.5	3.3	3.3
Heat productivity, A (μWm^{-3})	1.0	0.3	0	0
Friction angle[2], φ (°)	3; 30-6	30	30	30
Cohesion[2], C_0 (MPa)	1; 20-1	40	40	40
Bulk, shear modulus, K, G (GPa)[1]	55, 36	63, 40	122, 74	122, 74
Creep pre-exponential factor, Bd/Bn[3] (Pa^{-n}s^{-1})	-/8.57e-28	-/5.78e-27	1.5e-9/ 6.22e-16	1e-9/ 2.03e-15
Creep activation energy, Ed/En[3] (kJmol^{-1})	-/223	-/485	375/480	335/480
Creep activation volume Vd/Vn[3] (cm^{3}mol^{-1})	-/0	-/0	5/11	4/11
Power law exponent[3], n	-/4	-/4.7	1/3.5	1/3.5

[1]Temperature-dependent density: $\rho_{P,T} = \rho_0[1-\alpha\ (T-T_0)]$, where ρ_0 is the reference density at temperature T_0.

[2]Strain softening in the felsic crust via a decrease in φ and C_0 over the accumulated strain of 0.5 to 1.5. Sediment is assumed to be initially weak if it is 4-km-thick and φ is 3° and C_0 is 1 MPa.

[3]Viscous creep includes diffusion (Bd, Ed, Vd) and dislocation (Bn, En, Vn).

Mechanical boundaries include an open top surface and free-slip at the bottom boundary. The free surface stabilization approach (Kaus et al., 2010) is applied to the top boundary covered by the 10-km-thick low viscous and low density “sticky air” phase, which allows relatively large integration time step. Material flows in at a rate of 2 cm/year from the right-hand (East) side boundary and out at the left-hand side boundary beneath the orogenic lithosphere to maintain mass balance. The amount of shortening in our models (100 km) is appropriate and reasonable for shortening of the Central Andes over the last 10 Myr (Oncken et al., 2006; Horton, 2018). Moreover higher, but still reasonable shortening does not change main results (see **Figure S3** in the supporting information).

3 Model Results

3.1 Reference Model

In the reference model M1, the orogen has the same lithospheric structure as the foreland, except for the 4-km-thick sedimentary layer above the foreland, which differs from the upper crust only by density. After 100 km shortening, the felsic crust in both the orogen and its foreland undergoes pure-shear shortening, resulting in distributed crustal thickening and surface uplift (**Figure 2b**). **Figure 2c** shows that the strain rate norm (square root of the second invariant of deviatoric strain rate) is homogeneously distributed from the surface to the basement at ~17 km depth, and thus a fully thick-skinned tectonic style is formed in the foreland.

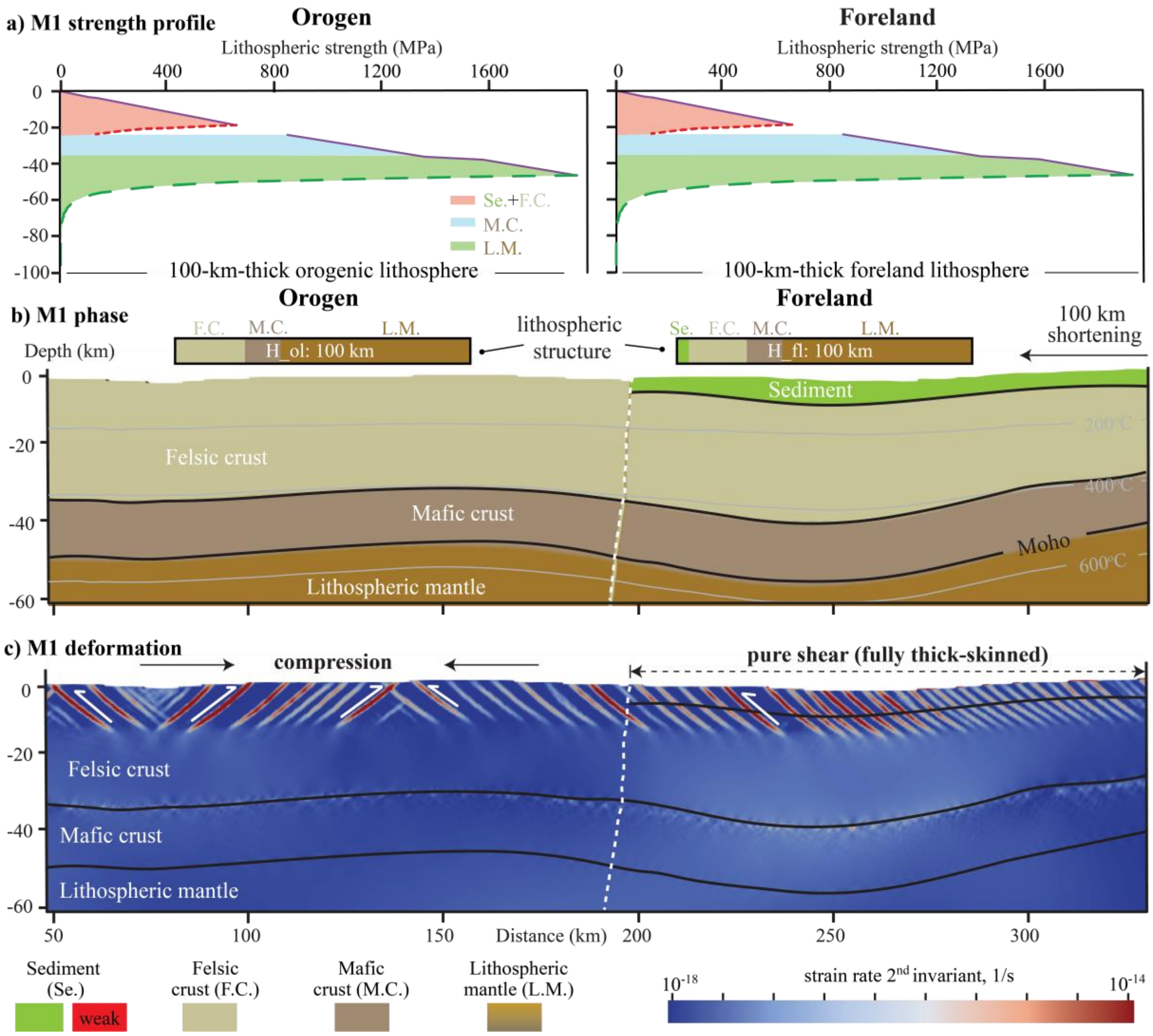

Figure 2. Reference model M1. **a)** Lithospheric strength profiles for both the orogen (left) and its foreland (right). **b)** and **c)** are model profiles of the phase and the deformation pattern after 100 km shortening, respectively. The two small bars above the phase profile are lithospheric structures of the orogen and foreland. Value of the lithospheric thickness (white) is inside them. Black line is the boundary between material phases. White one-way arrows represent the fault direction of the fault. Black dashed line with two arrows represents the thick-skinned tectonics in the foreland.

We conducted a series of modeling experiments that systematically investigate how the foreland-deformation pattern is affected by changes in the lithospheric structure, crustal structure, and foreland sedimentary strength (**Table 2**; also see **Figure S1** in the supporting information). Below we examine the effects of each of the following factors on the deformation style: (i) thickness of the orogenic lithosphere (H_ol); (ii) thickness of the orogenic crust (H_oc); (iii) thickness of the foreland lithosphere(H_fl); (iv) friction coefficient of foreland sediments (μ_se); (v) thickness of foreland sediments (H_se); and (vi) their combinations.

3.2 Variations in Orogenic and Foreland Lithospheric Structures

3.2.1 Orogenic Lithospheric Thickness and Orogenic Crustal Thickness

First, we fix the thickness of the orogenic crust as in the reference model (36 km) and change the thickness of the orogenic lithosphere. Geological and geophysical observations indicate that the lithosphere under some active orogens (e.g., the Central Andes) is thin or absent in the orogen-foreland compressional system (e.g., Beck & Zandt, 2002; Yuan et al., 2002). This is because the lithospheric mantle, being gravitationally unstable, is susceptible to removal via Rayleigh-Taylor-type instability (Molnar & Houseman, 2004) or delamination (Bird, 1979). In model M2 (**Figure 3a**), the orogenic lithosphere is as thin as 60 km and therefore weaker than the 100-km-thick foreland lithosphere. The model shows that the compressional deformation is localized within the orogen and its lithosphere is thickened after 100 km pure-shear shortening. Simultaneously, a fully thick-skinned structure is formed in the foreland. If the orogenic lithosphere is thicker and therefore stronger than the foreland lithosphere (e.g., M3), shortening is concentrated in the foreland with a fully thick-skinned structure. Therefore, in the models where only the orogenic lithospheric thickness changes, while the crustal thicknesses in the orogen and its foreland remain the same, shortening of the foreland crust is in pure-shear mode accompanied by the fully thick-skinned tectonic style.

When the orogenic crust is thickened to 60 km, the foreland crust underthrusts beneath the orogen regardless of the thickness of orogenic lithosphere within the range of parameters considered here (**Table 2**), which is interpreted as a simple-shear shortening mode. In this mode, if the contribution of the thin-skinned deformation to the total foreland crustal deformation is less than 10%, then we consider this tectonic style as thick-skinned dominated (e.g., M4 and M5). Compared to model M5, the orogenic lithosphere is thinner and much weaker in model M4 (see **Figure A1** for the strength contrast), and thus the foreland upper crust of model M4 underthrusts further towards the orogen, creating a larger viscous flow in the base of the thick orogenic crust. In both models, a pronounced deep detachment zone is produced between the upper crust and the lower crust in the foreland.

Table 2 List of the orogen-foreland shortening models. H_ol: thickness of the orogenic lithosphere, H_fl: thickness of the foreland lithosphere, H_oc: thickness of the orogenic crust, H_se: thickness of foreland sediments, μ_se = friction coefficient of foreland sediments; S. mode: shortening mode, S-1: pure-shear, S-2: simple-shear; T. style: tectonic style, T-1: fully thick-skinned, T-2: thick-skinned dominated, T-3: thin- & thick-skinned mixed, T-4: fully thin-skinned.

Models	Lithospheric thickness (km)		Crustal thickness (km)	Foreland sedimentary strength		Foreland-deformation pattern		Fig. #
	H_ol	H_fl	H_oc	H_se	μ_se	S. mode	T. style	
M1	100	100	36	4	0.5	S-1	T-1	2
M2	60	100	36	4	0.5	S-1	T-1	3a
M3	150	100	36	4	0.5	S-1	T-1	3b
M4	60	100	60	4	0.5	S-2	T-2	3c
M5	150	100	60	4	0.5	S-2	T-2	3d
M6	100	80	36	4	0.5	S-1	T-1	3e
M7	100	200	36	4	0.5	S-1	T-1	3f
M8	100	100	36	4	0.05	S-1	T-1	3g
M9	100	100	36	8	0.02	S-1	T-1	3h
M10	60	100	36	4	0.05	S-2	T-4	3i
M11	150	100	36	4	0.05	S-1	T-1	3j
M12	60	100	60	4	0.05	S-2	T-4	3k
M13	150	100	60	4	0.05	S-1	T-3	3l
M14	100	80	36	4	0.05	S-1	T-1	3m
M15	100	200	36	4	0.05	S-1	T-1	3n
M16	100	80	60	4	0.05	S-2	T-3	3o
M17	100	200	60	4	0.05	S-2	T-4	3p

3.2.2 Foreland Lithospheric Thickness

Here we test the effect of the foreland lithospheric strength on the deformation style by changing the foreland lithospheric thickness, while the initial crustal thicknesses in the foreland and the orogen are fixed. When the foreland lithosphere is 20 km thinner and thus weaker than the orogenic lithosphere (**Figure 4f**), the deformation mode in the foreland is pure-shear shortening with fully thick-skinned tectonics - same as in model M3. Unlike in the mountain belts, the foreland lithosphere in the craton area can be thicker than 150 km. For example, the thermal lithosphere is >180 km thick under some foreland regions of southwestern Canadian craton (Currie, 2016). In model M7, the thickness of the foreland cratonic lithosphere is 200 km thick and most of shortening is concentrated in the orogenic crust, resulting in crustal buckling and surface uplift. The fully thick-skinned structure is formed near the orogen-foreland boundary. As expected, the amount of the foreland deformation decreases with thickening of the foreland lithosphere.

3.2.3 Foreland Sedimentary Strength

The foreland sedimentary strength (coefficient of friction and its thickness) is also important for the foreland-deformation pattern. Here we test the value of the friction coefficient of foreland sediments from 0.5 in model M1 to 0.1-0.02 (e.g., M8 and M9), which is appropriate value of friction drop comparing with previous geodynamic models (e.g., Sobolev et al., 2006). The foreland deformation in model M8 is no longer homogenous as in the reference model; the pronounced thrust faults are produced in the middle part of the foreland (**Figure 3g**). When the friction coefficient of sediment is further reduced and its thickness increases (M9), the magnitude of deformation in the foreland increases and the fault system becomes more complicated. However, the shortening mode in these models remains pure-shear. There is also no underthrusting of the foreland crust and therefore the tectonic style is fully thick-skinned.

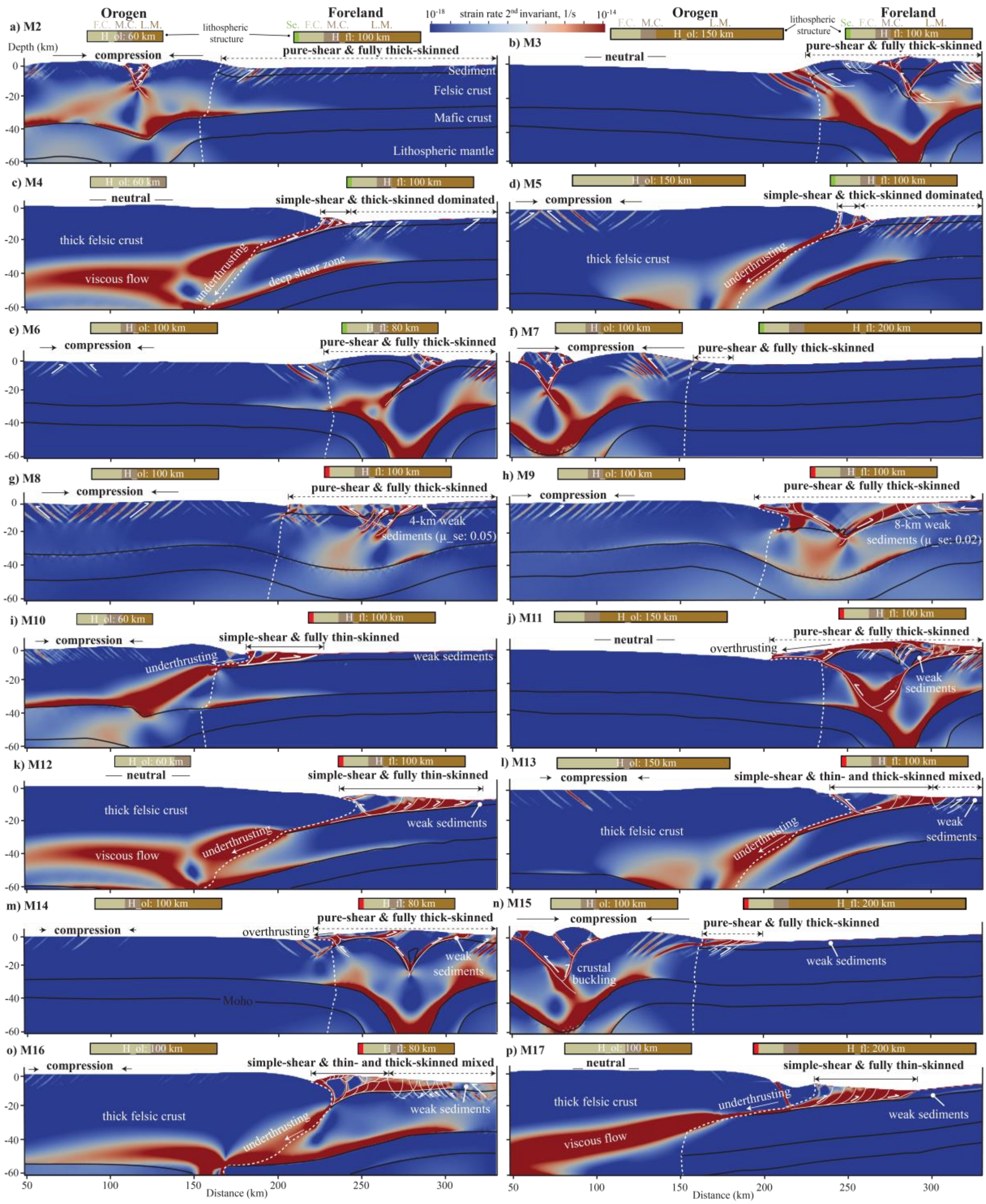

Figure 3. Foreland-deformation patterns in models M2-M17 after 100 km shortening. **a-h**) effects of individual factor and **i-p)** of multiple factors. Foreland sediments are considered as initially weak, i.e., red part in the foreland lithospheric structure bar, when its thickness is greater than 4 km and its

friction coefficient is not higher than 0.05. Black solid line with two arrows represents the thin-skinned tectonic style in the foreland.

3.2.4 Effects of Multiple Factors

None of the above models shows a wide thin-skinned thrust zone in the foreland. Here, we present models with the combination of multiple factors considered above (**Figure 3i-n**). All of these models have the 4-km-thick sedimentary layer in the foreland with a friction coefficient of 0.05 (we term "weak foreland sedimentary layer", i.e., red area in the lithospheric structure bar in **Figure 3**) while other model parameters are varied in the same way as in previous models. As we will see later, weak foreland sediments result in two additional tectonic styles, namely thin- and thick-skinned mixed and fully thin-skinned. We deem the tectonic style to be mixed if it combines features of both thin- and thick-skinned structures and its thin-skinned thrust zone is significantly wider than the zone in thick-skinned dominated tectonics (e.g., **Figure 3l, o**).

The weak sedimentary layer in most of the models facilitates the underthrusting of the foreland beneath the orogen and the development of mixed or fully thin-skinned tectonics (e.g., M12 and M13). The formation of the latter tectonic style further requires a relatively thick crust and thin lithosphere in the orogen (e.g., M12 and M17). Foreland weak sediments can also switch the shortening mode from pure-shear to simple-shear (e.g., compare M2 with M10) when the orogenic crust is thin (initially 36 km thick in these models) but the orogenic lithosphere is thinner than the foreland lithosphere. This switch does not occur if the orogenic lithosphere is thicker (e.g., compare M3 and M6 with M11and M14) or if the thicker foreland is in the craton zone (e.g., compare model M7 with M15). Additionally, these combined models show that large foreland underthrusting and the mid-crustal viscous flow leads to the orogenic crustal thickening and surface uplift.

4 Discussion

4.1 Lithospheric Strength Analysis

For each model, we calculated the initial integrated lithospheric strength of the orogen and its foreland as well as the strength ratio between them. The integrated strength is estimated through the integration of the yield strength envelope (e.g., Tesauro et al., 2013; Burov, 2011). Since the strength of the relatively thin sedimentary layer has little effect on the lithospheric strength, we neglect the strength change caused by the weakening of foreland sediments during the calculation. More details about the calculation are presented in **Appendix A**.

As we will show below, modeled deformation styles are first-order controlled by the difference in the lithospheric strength between the orogen and the foreland (**Figure 4**). We note, however, that the difference in the integrated strength of the entire lithosphere between the orogen and the foreland does not explain all model results. For example, the entire lithospheric strength of the orogen in model M13, including a 150-km-thick orogenic lithosphere and a 60-km-thick orogenic crust, is higher than that in model M18 with an 80-km-thick lithosphere and a 36-km-thick crust in the orogen (**Figure A1**, **S1**). Model M13 behaves in a simple-shear shortening with thin- and thick-skinned mixed structure in the foreland. As expected, when other parameters (i.e., the lithospheric strength and the foreland sedimentary strength) are fixed, and only the orogenic lithosphere is weaker than the foreland lithosphere, the foreland crust underthrusts beneath the orogen further and causes a larger amount of thin-skinned deformation (e.g., compare M12 with M13). However, the model behavior of M18 is contradictory to this view, where the tectonic type is thick-skinned dominated with a narrow thin-skinned wedge zone on the edge of the foreland (**Figure S1**).

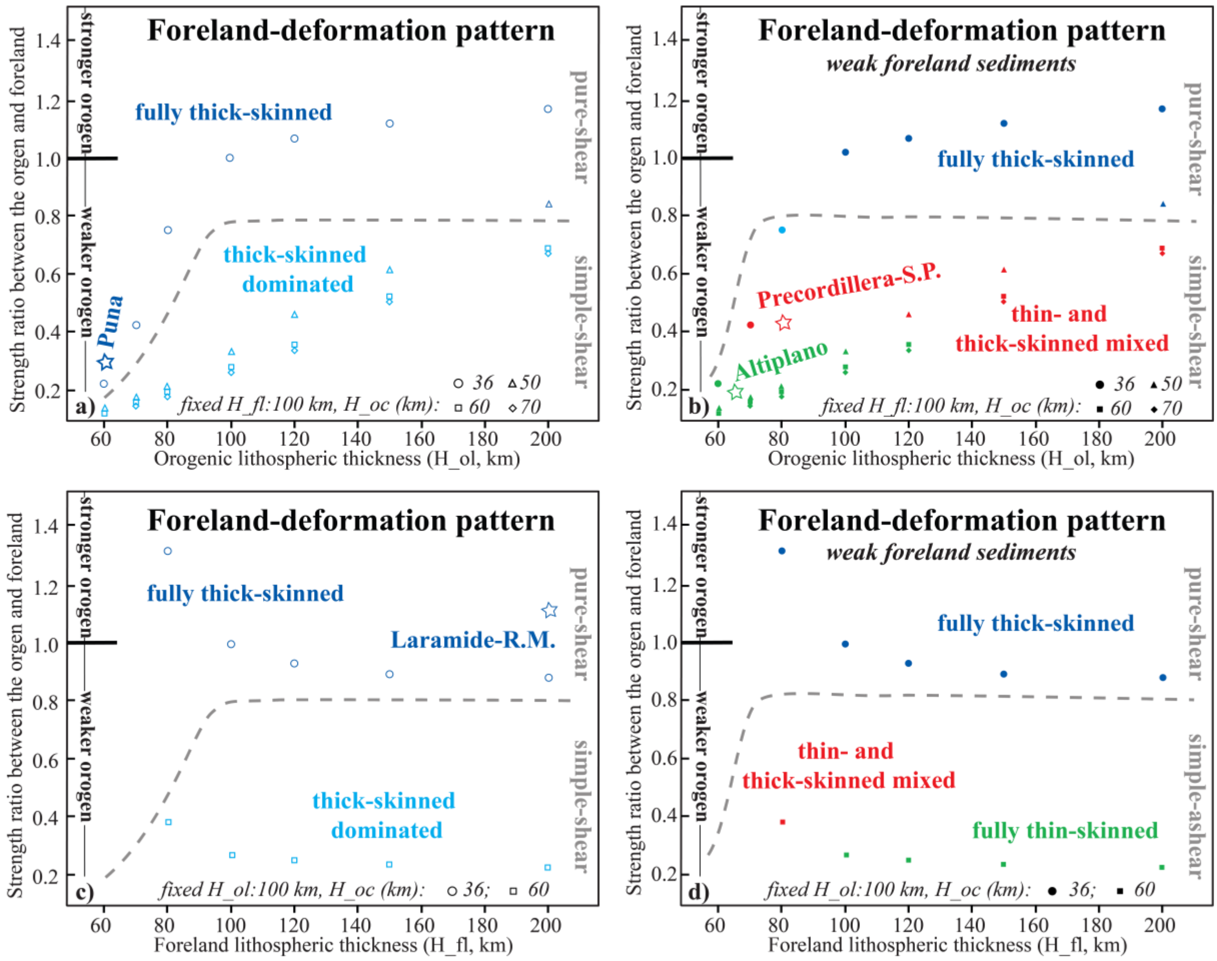

Figure 4. Foreland-deformation patterns **a, c)** without or **b, d)** with weak foreland sediments. **a-b)** and **c-d)** represent the changes in the orogenic lithospheric thickness and in the foreland lithospheric thickness, respectively. The orogen is stronger than the foreland when the ratio >1. Four different

tectonic styles are fully thick-skinned (dark blue), thick-skinned dominated (light blue), thin- and thick-skinned mixed (red), and fully thin-skinned (green). Grey dashed curve shows the presumptive transition between the two shortening modes. Hollow stars indicate four natural systems with different foreland-deformation patterns. R.M. - Rocky Mountains; S.P. - Sierras Pampeanas.

Figure 4 shows that strength difference of the upper part of the lithosphere between the orogen and its foreland control the foreland-deformation pattern better than the strength difference of the entire lithosphere. With this new definition of the upper lithospheric strength model M18 has a higher strength ratio than model M13, i.e., model M18 has a stronger upper orogenic lithosphere than model M13. As a result, less thin-skinned deformation is formed in model M18.

If the upper lithospheric strength in the orogen and its foreland are similar (strength ratio ~0.8-1.3 in **Figure 4**), then the foreland (and the orogen) should deform in a pure-shear mode accompanied by the thick-skinned deformation. Less obvious is foreland simple-shear shortening and thin-skinned tectonics at a low strength ratio, i.e., when the orogenic lithosphere is much weaker than the foreland lithosphere. In this case, the intuitive scenario would be the localization of shortening in the weak orogen rather than in the foreland. However, the strong foreland in our models behaves in different deformation patterns. We infer that in addition to the lithospheric strength mentioned above, the gravitational potential energy (GPE) of the orogen also contributes to the foreland-deformation pattern.

Generally, the compressive force driving the orogenic shortening (i.e., the mountain building) causes the thickening of the orogenic crust. During shortening, the force works against two mainly resistive forces, which are the mechanical strength (discussed in this study) and the gravity (e.g., Molnar & Lyon-Caen, 1988). The work against the gravity creates the gravitational potential energy. The GPE per unit surface of the Earth area in the orogen increases with crustal thickening. Thus, to shorten the orogen further, it requires an increasingly larger amount of work from the driving force to overcome the increasing GPE. When the force can no longer supply the energy needed to elevate the orogen higher, the mountain range is likely to grow laterally in width instead of increasing in height and crustal thickness (Molnar & Lyon-Caen, 1988). Consequently, when the orogen grows laterally, the work done by the specified driving force will be used for deforming the orogenic edge and its foreland, even if the orogenic lithosphere is much weaker than the foreland lithosphere. In this scenario, the foreland lithosphere can underthrust beneath the edge of the orogen, i.e., the foreland shortening mode is simple-shear (**Figure 4**). If there is a thick layer of mechanically weak sediments in the foreland, then shear deformation is localized in the sedimentary layer and the foreland tectonic style is thin-skinned (**Figure 4b, d**). In this study, we treat the role of GPE as a qualitative reasonable assumption without testing its effect on lithospheric strength, because the GPE of the orogen is in turn controlled by its crustal thickness and lithospheric thickness.

4.2 Structural Controls on the Shortening Mode and Tectonic Style in the Foreland

Our model results demonstrate that the variation of the orogenic strength caused by the change in the orogenic crustal thickness has a critical effect on controlling the shortening mode. Pure-shear mode develops in the models with little difference in the crustal thickness between the orogen and the foreland, while the thickened orogenic crust is required to switch from pure-shear to simple-shear (**Figure 4**). The thickened orogenic crust causes the initially high GPE of the orogen and low strength of the orogenic upper lithosphere. This high GPE forces tectonic shortening in the foreland while the thick and weak orogenic crust allows the strong foreland lithosphere to easily intrude into it easily in simple-shear mode. Our models show that other four individual factors (H_ol, H_fl, μ_sed and H_sed) have little effect on the transition of shortening mode with one exception. That is the case (the dashed rectangular in **Figure S1**) when the orogenic crust is much thicker (high GPE) than the foreland crust and the foreland lithosphere is thin, showing a pure-shear shortening mode in the foreland.

Our models show that significantly lower strength of the upper lithosphere in the orogen than in the foreland (strength ratio < ~0.7) and the presence of thick and weak foreland sediments are responsible for the thin-skinned tectonics in the foreland. Absence of these conditions results in the tectonic style of fully thick-skinned or thick-skinned dominated. Furthermore, the condition of thick and weak foreland sediments generally intensifies simple-shear shortening by making underthrusting easier and thus broadening the thin-skinned thrust zone. When the orogenic crust is thick and the foreland lithosphere is thin, this condition can even switch the shortening mode in the foreland from pure-shear to simple-shear.

4.3 Applications to Natural Orogen-Foreland Shortening Systems

Here, we compare our model inferences to the Central and Southern Andes and the Laramide Orogeny, and provide a first-order fit of the foreland-deformation pattern to these natural shortening systems. We will look more specifically at the Altiplano-Puna plateau-foreland profile (**Figure 5b-c**), the Frontal Cordillera-Precordillera-Sierras Pampeanas profile (**Figure 5d**), and a more conceptual cross-section through the Colorado Plateau and Southern Rocky Mountain foreland (**Figure S4**).

4.3.1 Altiplano-Puna Plateau

In the Central Andes, the Altiplano-Puna Plateau was formed with an N-S oriented deformation diversity, including a broad wedge-shaped thin-skinned thrust belt in the Interandean-Subandean zone and the thick-skinned structure in the Santa Barbara System (**Figure 5a**). The lithosphere under the plateau is very thin, but the upper felsic crust is as thick as 50-70 km (e.g., Tassara et al., 2006; Ibarra et al., 2019). This inherited thin lithosphere is suggested to be the result of lithosphere delamination, which occurred during Cenozoic shortening (e.g., Kay & Kay, 1993; Beck & Zandt, 2002; Sobolev & Babeyko, 2005; Kay & Coira, 2009). The Puna Plateau and its foreland area have a higher seismic attenuation, implying a hotter and thinner lithosphere than the northern Altiplano part (Whitman et al., 1996). Paleozoic and Mesozoic sediments abundantly deposited in the Subandean zone but pinch out southward to the Santa Barbara system (e.g., Allmendinger & Gubbels, 1996; Pearson et al., 2013). The local wet condition in the foreland since the late Cenozoic (Strecker et al., 2007) indicate abundant fluids are stored in these ancient sediments and may weaken them by increasing their pore fluid pressure.

We applied these observations to the case of the Central Andes. In the models (**Figure 5b-c**), the thickness of the orogenic crust under the Altiplano-Puna Plateau is 60 km and an additional 10-km-thick lithospheric mantle is attached to the Altiplano crust. The orogenic lithosphere under the Puna Plateau only contains the thick crust due to mantle lithosphere delamination. The lithosphere of the Puna foreland in the model is 70-km-thick, 30 km thinner than the Altiplano foreland lithosphere. In agreement with observations, the weak sedimentary layer in the model covers only the north Altiplano foreland crust (**Figure 5b**). Model results clearly show that the simple-shear mode with a fully thin-skinned thrust belt and the pure-shear mode with the fully thick-skinned structure are formed in the Altiplano foreland and the Puna foreland, respectively. Our models not only support and specify the results of previous relatively low-resolution modeling studies (e.g., Babeyko & Sobolev, 2005), but also reproduce observed east-dipping reverse faults in the foreland edge in both cases.

4.3.2 Precordillera-Sierras Pampeanas Region

The Sierras Pampeanas province, located on the eastern side of the Precordillera thin-skinned thrust belts, is known as a modern analog of the thick-skinned deformation of the Laramide province (Jordan & Allmendinger, 1986). The tectonic style of the Precordillera-Sierras Pampeanas foreland region, adjacent to the Frontal Cordillera, can be broadly considered as thin- and thick-skinned mixed structure (**Figure 5a**). The oceanic flat-slab below the Frontal Cordillera stays at 100 km depth, and thus, the orogenic lithosphere of the Frontal Cordillera may be less than 100 km thick (e.g., Jordan et al., 1983; Ramos & Folguera, 2009). The lithospheric thickness increases eastward and is more than 20 km thicker in the Sierras Pampeanas foreland. Crustal thickness exceeds 60 km beneath the Frontal Cordillera and rapidly decreases eastward to less than 40 km below its foreland (e.g., Ramos et al., 2004; Perarnau et al., 2012). Furthermore, there are abundant Paleozoic sedimentary rocks in the Precordillera whereas only a small amount of Cenozoic sediments covers the Sierras Pampeanas (e.g., Ramos et al., 2004; Meeßen et al., 2018).

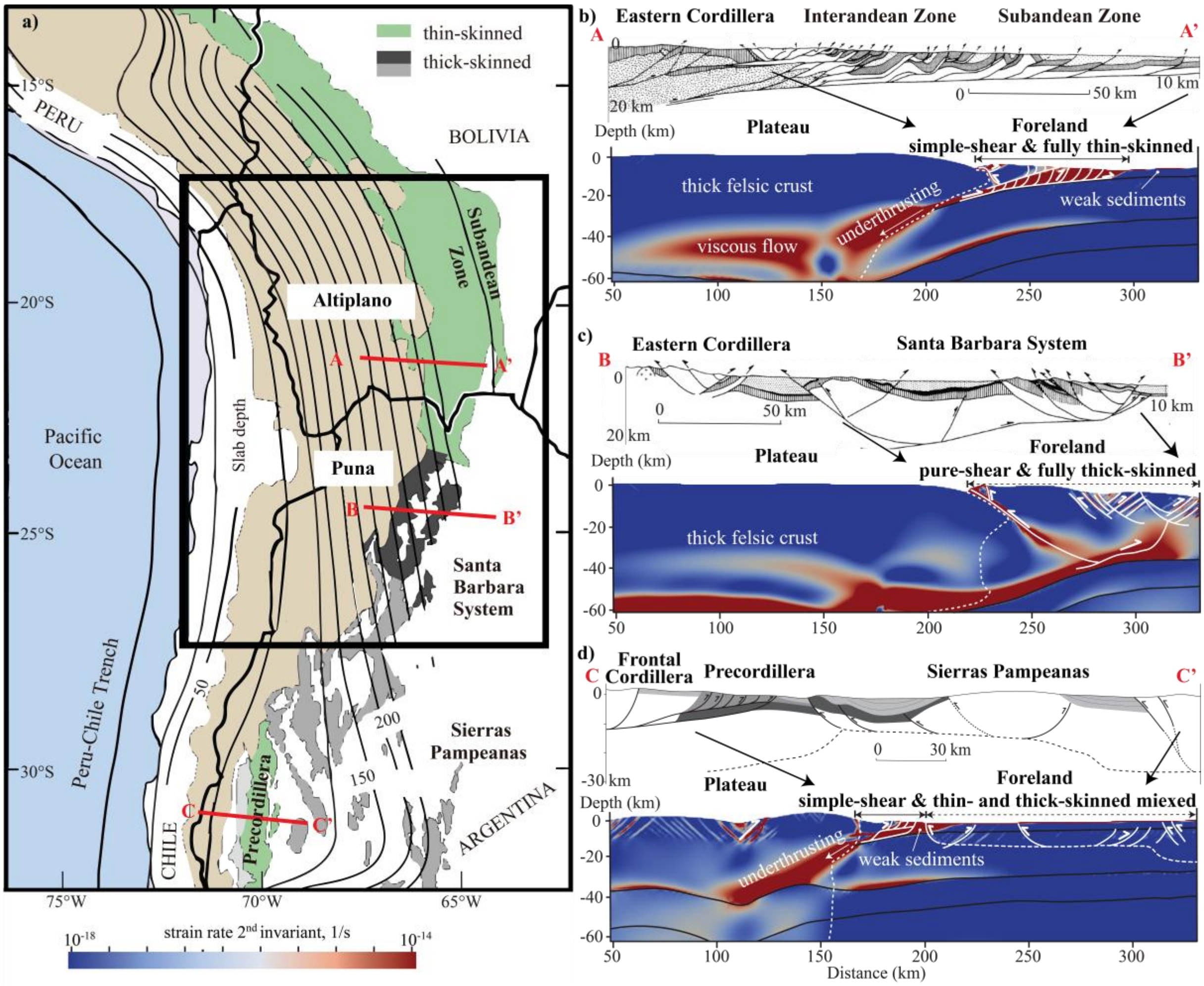

Figure. 5. Numerical models with application to the cases of the Central and Southern Andes. **a)** is the simple tectonic map modified from Kay & Coira (2009). The tan area shows the elevation above 3.7 km. Geological structures of two cross-sections A-A' and B-B' are modified from Kley et al. (1999), showing **b)** fully thin-skinned tectonics in the Interandean-Subandean zone and **c)** fully thick-skinned tectonics in the Santa Barbara system. Crustal-scale cross-section C-C' is modified from Siame et al. (2006), Bellahsen et al. (2016), and Mescua et al. (2016), showing **d)** the tectonic style of thin- and thick-skinned mixed in the Precordillera-Sierras Pampeanas system.

Unlike the 30°-dipping subducted slab in the Central Andean case, the slab in the southern Argentine Andean case is nearly horizontal (Jordan et al., 1983; Gutscher et al., 2000). Slab flattening can enhance the stress transmission from the subducting plate into the overlying plate by increasing the degree of plate coupling (e.g., Lacombe & Bellahsen, 2016), thus promoting the plateau-foreland shortening, which may contribute to the development of thick-skinned tectonics (see next section for details). Note, however, that in the cases of the Sierras Pampeanas and the Laramide below, we do not introduce the factor of flat-slab subduction, therefore our models do not fully reproduce amount of shortening and high topography of these two provinces.

The model constrained by these observations includes a thin and weak orogenic lithosphere that is 30 km thinner than the foreland lithosphere. Crustal thickness is greater than 60 km in the orogen and decreases to ~ 40 km in the foreland. The model result (**Figure 5d**) indicates that a simple-shear shortening occurs in the foreland, accompanied by mixed tectonics consisting of thin-skinned thrust at the foreland edge (Precordillera) and thick-skinned structure behind (Sierras Pampeanas). Note that the weak sedimentary layer is located through the entire foreland area in our model. Although here it has little influence on the tectonic style of the Sierras Pampeanas, it is necessary to consider the difference of sedimentary thickness between the Precordillera and Sierras Pampeanas in future studies.

4.3.3 Laramide Province

The Laramide province (i.e., the Rocky Mountain foreland adjacent to the Colorado Plateau) is a widely thick-skinned deformation zone that developed more than 1000 km inboard from the plate margin (e.g., Bird, 1984; Saleeby 2003; Erslev, 2013; Yonkee & Weil, 2015; Lacombe & Bellahsen, 2016). This province sustained more than 100 km pure-shear shortening, which contrasts strongly with minor deformation of the Colorado Plateau (e.g., Bird, 1984; Spencer 1996; Flowers et al., 2008; Humphreys, 2009). Dynamic processes that propagate deformation across the strong and broad plateau far into the foreland and produce thick-skinned tectonics in the case of the Laramide Orogeny are still largely debated.

One fashionable possibility is that the formation of the Laramide province is suggested to be the result of slab flattening of the Farallon plate. In particular, this process enhanced interplate coupling along the base of the cratonic lithosphere root, hence efficient stress transmission from the Farallon plate into the North American plate to deform the plateau-foreland system (e.g., Bird 1984; Axen et al., 2018). Furthermore, flat-slab subduction likely changed the strength of the continental lithospheric mantle. For instance, a cold slab can cool the above basal lithospheric mantle, which favors increased strength and stress transfer far into the foreland. In contrast, the lithospheric mantle can also be weakened as a result of effects of basal lithospheric mantle removal by flat-slab subduction (e.g., Bird, 1984; Liu & Currie, 2016; Axen et al., 2018), hydration from dewatering of the underlying flat-slab and heating by magmatic ascent (Humphreys et al., 2003), and/or thermal inheritance from the pre-orogenic extension (Marshak et al., 2000). Lithospheric mantle weakening may allow shortening to occur in the deep mantle beneath the southern Rocky Mountains. This process, together with enhanced stress transfer, possibly promotes crustal shortening and leads to thick-skinned deformation within the foreland.

In addition to the flat-slab subduction, crustal/lithospheric buckling has been considered to be another possible mechanism for propagating and accommodating deformation in the Laramide foreland (e.g., Erslev, 1993; Tikoff & Maxson, 2001; Lacombe and Bellahsen, 2016 and reference therein). For instance, Lacombe and Bellahsen (2016) emphasize that thick-skinned tectonics in the orogenic foreland is favored by the occurrence of a ductile middle or lower crust of a young, and hot lithosphere, hence enabling crust-mantle decoupling. Depending on its composition - felsic or mafic granulites - the middle or lower crust may have been either moderately weak with potential concentration of ductile flow along deep décollements or strong with potential for lithospheric buckling (Yonkee & Weil, 2015). Overall, intervening specific boundary conditions such as flat-slab subduction, together with structural crustal inheritance and possible mantle weakening, may provide a sophisticated explanation for intraplate basement-involved shortening in the Laramide setting.

As the deformation did not propagate regularly in a classical ‘in sequence’, foreland-ward way from the former Sevier orogen to the Laramide orogen, individual basement-cored deformation zones in the Laramide province may have developed spatially and temporally in a rather complex sequence (e.g., Crowley et al., 2002; Lacombe & Bellahsen, 2016). Since we are concentrated with the foreland-deformation pattern during the Laramide Orogeny, here we simply developed a conceptual plateau-foreland shortening model constrained by observations of an SW-NE tectonic transect through the Colorado Plateau and Southern Rocky Mountain foreland, which does not include the Sevier Orogeny (**Figure S4** in the supporting information). Although both the western Farallon flat-slab subduction and eastern intraplate shortening between the Colorado Plateau and the Rocky Mountain foreland can happen during the Laramide deformation, we focus on the latter event and the subduction process is not integrated in the Laramide shortening model. Alternatively, we suppose that the presumptive flat-slab subduction on the left boundary prevents the leftward motion of the plateau, so we close the left boundary above the orogenic lithosphere, which may result in a high degree of coupling between the plateau and its foreland.

In this transect, the Colorado Plateau and nearby Rocky Mountain foreland presumably involved a cool and thick lithosphere at the time of the Laramide Orogeny. The xenolith-based observations estimate the lithospheric thickness of the Colorado Plateau to be more than 150 km due to its underlying cold, refractory mantle root (e.g., Smith & Griffin, 2005; Li et al., 2008). Previous numerical studies of the flat-slab subduction suggest that the Colorado Plateau may be thicker and thus stronger than its foreland cratonic lithosphere due to its deep cratonic root (e.g., O'Driscoll et al., 2009; Liu & Currie, 2016). The foreland was formerly part of a continental platform with an approximately 33-km-thick crust before the Laramide Orogeny (Bird, 1984). The difference in the crustal thickness between the orogen and its foreland is less than 5 km (Das & Nolet, 1998). The lower crust is cool, viscous, and largely intact beneath the Colorado Plateau (Humphreys et al., 2003). Lithostratigraphic columns of Laramide sedimentary successions in depocenters of key Laramide basins show that thickness of the sedimentary cover is not more than 4 km (Dickinson et al., 1988).

Here, we apply model M3 (**Figure 3b**, **S2**) to the Laramide case. In this model, the plateau lithosphere is thicker and stronger than the foreland lithosphere and there is little difference of crustal structure between them. Moreover, the value of strength ratio between the orogen and its foreland in this model is very close to the value calculated from the Laramide case (the hollow star of the Laramide-R.M. case in **Figure 4c**).

The results of M3 may likely agree with the first-order observed foreland-deformation pattern in the Laramide province. When the strength of the upper lithosphere of the orogen is slightly greater than that of the foreland and their crustal structures are not much different, the foreland is subjected to pure-shear shortening with fully thick-skinned tectonics (**Figure 3b**), and there is minor deformation in the plateau. The foreland deformation is mainly accommodated in the felsic upper-middle crust, which could potentially imply decoupling between felsic upper-middle crust and mafic lower crust and lithospheric mantle. Our model results support the mechanism of lithospheric buckling in the Laramide deformation.

Note that we have not attempted to provide a thorough review of the Andean/Laramide orogeny. Rather, we have attempted to demonstrate that the foreland-deformation pattern of the Andean/Laramide orogeny is consistent with simplified orogen-foreland shortening models. The very fine internal structure of the deformed sediments is not well visible in our models and is modelled as a zone with the finite strain more than 1. This is because our models did not employ a deformed mesh used in Erdős et al. (2015) and Jammes and Huismans (2012), although the resolution of our models is sufficient. We have addressed only the contrast in the lithospheric strength between the orogen and foreland and strength of the foreland sediment within these shortening models. Other parameters (e.g., the rate and amount of shortening, subduction dynamics, and thermal/structural inheritance) have not been addressed here but are necessary to be considered in future comprehensive case studies.

5 Conclusions

With high-resolution thermomechanical numerical models, we systematically examine the effects of the lithospheric structure and foreland sedimentary strength on the foreland-deformation pattern subjected to tectonic shortening.

We find that three factors significantly control the shortening mode (pure-shear or simple-shear) and the tectonic style (thick-skinned or thin-skinned): (i) the strength difference in the upper lithosphere between the orogen and its foreland, rather than the difference in the entire lithospheric strength between them; (ii) GPE of the orogen that is in turn controlled by its crustal thickness and lithospheric thickness, and (iii) the strength and thickness of the deforming foreland sediments.

If the strength of the orogenic upper lithosphere is higher or similar to that of the foreland upper lithosphere (strength ratio > ~0.8) and the orogenic crust is not much thicker than the foreland crust (relatively low GPE of the orogen), a pure-shear shortening develops in the foreland.

If the strength of the orogenic upper lithosphere is significantly lower than that of the foreland upper lithosphere (strength ratio < ~0.7) and the orogenic crust is much thicker than the foreland crust (> 50 km causing relatively high GPE of the orogen), foreland undergoes a simple-shear shortening.

In the particular case of a thick orogenic crust (> 50 km, high GPE) and thin (< 70 km) orogenic lithosphere, and simultaneously thin (< 70-80 km) foreland lithosphere, the foreland shortening mode is pure-shear (Puna-Santa Barbara system case).

Fully thin-skinned or thin- & thick-skinned mixed tectonic style can develop in the foreland only if thick (> ~4 km) and mechanically weak (friction coefficient < ~0.05) sediments are present in the simple-shear shortening mode. Further, the most pronounced fully thin-skinned tectonics develops in the thick and weak foreland sedimentary layer when the strength of the orogenic upper lithosphere is much lower than that of the foreland upper lithosphere (strength ratio < 0.3-0.4; Altiplano-Subandean ranges case).

Our high-resolution orogen-foreland shortening models successfully reproduce foreland-deformation patterns in the Central and Southern Andes in South America during the Neogene and Laramide Province in North America during the Late Cretaceous to Paleocene.

Acknowledgements

The research is within the framework of the project *IGK 2018 SuRfAce processes, Tectonics and Georesources*: *The Andean foreland basin of Argentina* (StRATEGy) and funded by the Deutsche Forschungsgemeinschaft (DFG, grant STR 373/34-1) and the Brandenburg Ministry of Sciences, Research and Cultural Affairs, Germany. Computations were performed with resources provided by the North-German Supercomputing Alliance (HLRN). Input files used to produce the results in this work are available at https://github.com/sibiaoliu/paper-Orogen-Foreland-Shortening-System. We thank Peter van der Beek, Olivier Lacombe, Zoltán Erdős and one anonymous reviewer for their thoughtful suggestions on an earlier revision of this manuscript.

Appendix A: Geodynamic Governing Equations and Yield Strength Envelope

Material deformation is governed by solving the coupled system of momentum (1), mass (2), and energy (3) conservation equations below:

$$\frac{\partial \tau_{ij}}{\partial x_j} - \frac{\partial P}{\partial x_i} + \rho g_i = 0 \quad (1)$$

$$\frac{1}{K}\frac{DP}{Dt} - \alpha\frac{DT}{Dt} + \frac{\partial v_i}{\partial x_i} = 0 \quad (2)$$

$$\rho C_p \frac{DT}{Dt} = \frac{\partial}{\partial x_i}\left(k\frac{\partial T}{\partial x_i}\right) + \tau_{ij}\left(\dot{\varepsilon}_{ij}^{v} + \dot{\varepsilon}_{ij}^{p}\right) + \rho A \quad (3)$$

where i, j represent spatial directions following Einstein summation convention, $x_{i,j}$ are the Cartesian coordinates, τ_{ij} is the deviatoric stress tensor, P is pressure, ρ is the density, g_i is the gravitational acceleration vector, v_i and v_j are components of the velocity, D/Dt is the material time derivative, K is bulk modulus, α is the thermal expansion coefficient, C_p is specific heat, k is thermal conductivity, A is the radiogenic heat production, and $\dot{\varepsilon}_{ij}^{v}$, $\dot{\varepsilon}_{ij}^{p}$ are viscous and plastic strain-rate deviators, respectively. Repeated indices imply summation. These basic geodynamic equations are solved assuming plane strain, incompressibility, and neglecting thermal diffusion.

The material behaves the frictional-plastic deformation when the deviatoric stress exceeds the plastic yield stress (τ_Y), which follows a pressure-dependent Drucker-Prager yield criterion:

$$\tau_Y = P \sin\varphi + C_0 \cos\varphi \qquad (4)$$

where φ is the internal friction angle and C_0 is the cohesion. Here we assume the friction coefficient $\mu = tan(\varphi)$. Below this yield stress, materials deform viscously with an effective viscosity (η_{eff}) given by:

$$\eta_{eff} = \frac{1}{2B^{1/n}} \dot{\varepsilon}_{II}{}^{(1-n)/n} \exp\left(\frac{E+PV}{nRT}\right) \qquad (5)$$

where $\dot{\varepsilon}_{II} = \sqrt{\frac{1}{2}\dot{\varepsilon}_{ij}\dot{\varepsilon}_{ij}}$ is the second invariant of the square root of the deviatoric strain rate, $\dot{\varepsilon}_{ij} = \frac{1}{2}\left(\frac{\partial V_i}{\partial x_j} + \frac{\partial V_j}{\partial x_i}\right)$, R is the gas constant. B, n, E, V are the laboratory-derived pre-exponential viscosity parameter, stress exponent, activation energy and activation volume, respectively.

<u>**Integrated strength of the lithosphere**</u> (σ_L) under compression is estimated from the yield strength envelope (YSE):

$$\sigma_L = \int_0^h (\sigma_1 - \sigma_3) dz = \int_0^h \min(\sigma_B,\ \sigma_D) dz \qquad (6)$$

where h is the lithospheric thickness and σ_1 and σ_3 are the maximum and minimum principal stress component, respectively. **Figure A1** shows initial strength envelopes of the lithosphere with different structures. There are two different types in the envelope: the frictional brittle strength (σ_B; solid purple line in **Figure A1**) and the ductile strength (σ_D; dashed colored curves in **Figure A1**). The brittle strength is estimated by the Byerlee's law (Byerlee, 1978) and a function of pressure independent of rock type in a compressional environment: $\sigma_B = \int_0^h 2\mu(\sqrt{\mu^2+1} + \mu)\rho g(1-\lambda) dz$, where λ, the pore fluid factor, equals to 0.36. $\sigma_D = (\frac{\dot{\varepsilon}_{ref}}{B})^{\frac{1}{n}} \exp\left(\frac{E+PV}{nRT}\right)$, where $\dot{\varepsilon}_{ref}$ is the initial reference strain rate (10^{-16} s^{-1}) and viscous parameters are corresponding to the dislocation creep mechanism from laboratory measurements.

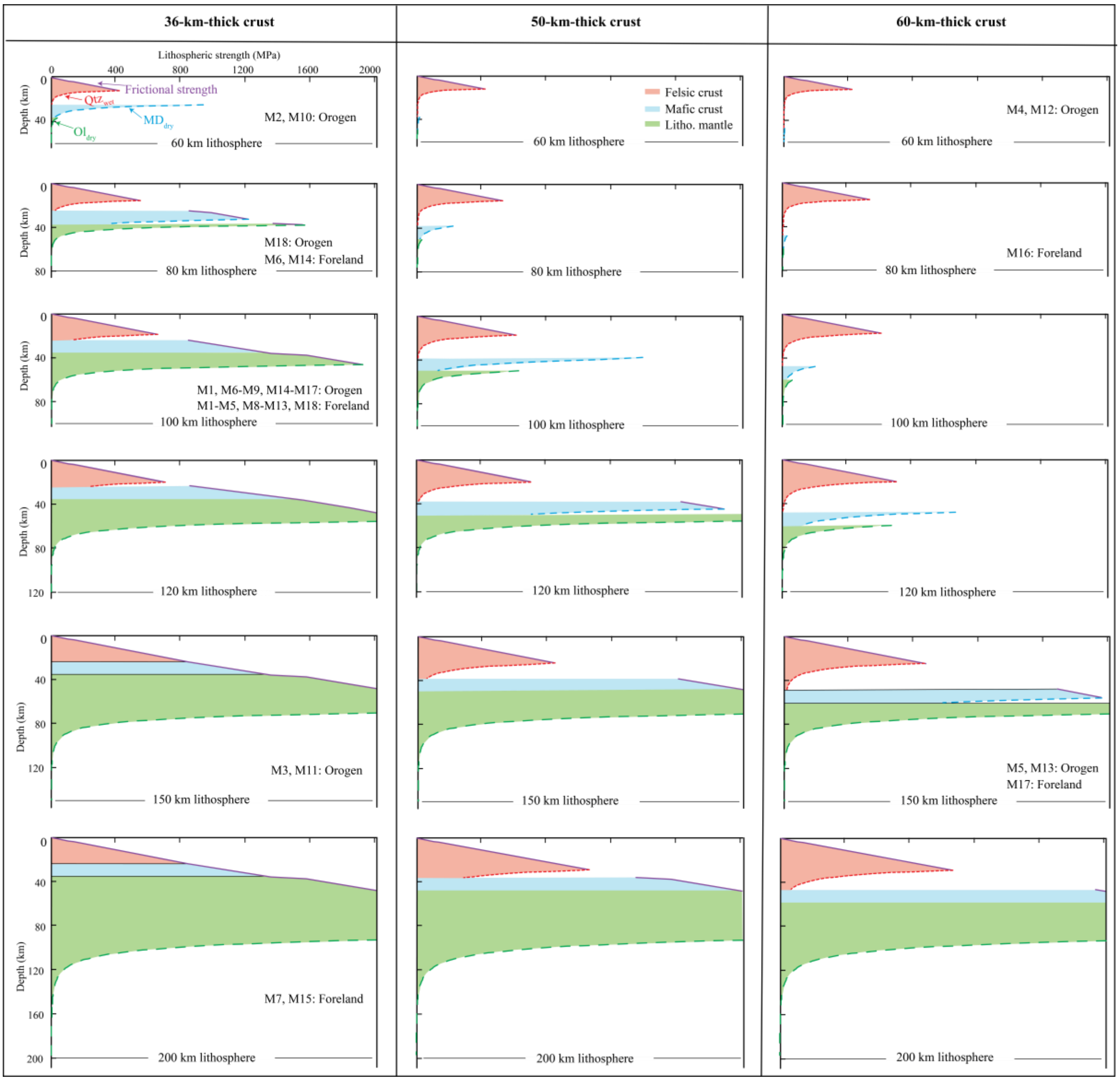

Figure A1. List of strength profiles for different initial lithospheric structures (60-200 km) and crustal structures (36-60 km). Lithospheric strengths of the orogen and its foreland for each model mentioned above are shown. For example, M1-M5: Foreland, means the initial 100-km-thick lithospheric strength of the foreland in models M1 to M5.

References

Allmendinger, R. W., & Gubbels, T. (1996). Pure and simple shear plateau uplift, Altiplano-Puna, Argentina and Bolivia. *Tectonophysics*, *259*(1), 1–13. https://doi.org/10.1016/0040-1951(96)00024-8.

Axen, G. J., van Wijk, J. W., & Currie, C. A. (2018). Basal continental mantle lithosphere displaced by flat-slab subduction. *Nature Geoscience*, *11*(12), 961–964. https://doi.org/10.1038/s41561-018-0263-9.

Babeyko, A. Y., & Sobolev, S. V. (2005). Quantifying different modes of the late Cenozoic shortening in the central Andes. *Geology*, *33*(8), 621–624. https://doi.org/10.1130/G21126AR.1.

Babeyko, A. Y., Sobolev, S. V., Vietor, T., Oncken, O., & Trumbull, R. B. (2006). Numerical Study of Weakening Processes in the Central Andean Back-Arc. In O. Oncken, G. Chong, G. Franz, P. Giese, H.-J. Götze, V. A. Ramos, et al. (Eds.), *The Andes* (pp. 495–512). Springer Berlin Heidelberg. Retrieved from http://link.springer.com/10.1007/978-3-540-48684-8_24.

Barrionuevo, M., Liu, S., Mescua, J., Yagupsky, D., Quinteros, J., Giambiagi, L., Sobolev, S. V., Piceda, C. R., Strecker, M. R. (2021). The influence of variations in crustal composition and lithospheric strength on the evolution of deformation processes in the southern Central Andes: insights from geodynamic models. International Journal of Earth Sciences, 110(7), 2361–2384.

Beck, S. L., & Zandt, G. (2002). The nature of orogenic crust in the central Andes. *Journal of Geophysical Research: Solid Earth*, *107*(B10), ESE 7-1-ESE 7-16. https://doi.org/10.1029/2000JB000124.

Bellahsen, N., Mouthereau, F., Boutoux, A., Bellanger, M., Lacombe, O., Jolivet, L., & Rolland, Y. (2014). Collision kinematics in the western external Alps. *Tectonics*, *33*(6), 1055–1088. https://doi.org/10.1002/2013TC003453.

Bellahsen, N., Sebrier, M., & Siame, L. (2016). Crustal shortening at the Sierra Pie de Palo (Sierras Pampeanas, Argentina): near-surface basement folding and thrusting. *Geological Magazine*, *153*(5–6), 992–1012. https://doi.org/10.1017/S0016756816000467.

Bird, P. (1979). Continental delamination and the Colorado Plateau. *Journal of Geophysical Research: Solid Earth*, *84*(B13), 7561–7571. https://doi.org/10.1029/JB084iB13p07561.

Bird, P. (1984). Laramide crustal thickening event in the Rocky Mountain Foreland and Great Plains. *Tectonics*, *3*(7), 741–758. https://doi.org/10.1029/TC003i007p00741.

Brown, D., Alvarez-Marrón, J., Pérez-Estaún, A., Gorozhanina, Y., Baryshev, V., & Puchkov, V. (1997). Geometric and kinematic evolution of the foreland thrust and fold belt in the southern Urals. *Tectonics*, *16*(3), 551–562. https://doi.org/10.1029/97TC00815.

Burov, E. B., & Watts, A. B. (2006). The long-term strength of continental lithosphere: jelly-sandwich or crème-brûlée?. *GSA Today*, *16*(1), 4-10. https://doi.org/10.1130/1052-5173(2006)016<4:TLTSOC>2.0.CO;2.

Burov, E. B. (2011). Rheology and strength of the lithosphere. *Marine and Petroleum Geology*, *28*(8), 1402–1443. https://doi.org/10.1016/j.marpetgeo.2011.05.008.

Byerlee, J. (1978). Friction of rocks. *Pure and Applied Geophysics*, *116*(4–5), 615–626. https://doi.org/10.1007/BF00876528.

Cloetingh, S., & Burov, E. B. (1996). Thermomechanical structure of European continental lithosphere: constraints from rheological profiles and EET estimates. *Geophysical Journal International*, *124*(3), 695–723. https://doi.org/10.1111/j.1365-246X.1996.tb05633.x.

Cobbold, P. R., Mourgues, R., & Boyd, K. (2004). Mechanism of thin-skinned detachment in the Amazon Fan: assessing the importance of fluid overpressure and hydrocarbon generation. *Marine and Petroleum Geology*, *21*(8), 1013–1025. https://doi.org/10.1016/j.marpetgeo.2004.05.003.

Crowley, P. D., Reiners, P. W., Reuter, J. M., & Kaye, G. D. (2002). Laramide exhumation of the Bighorn Mountains, Wyoming: An apatite (U-Th)/He thermochronology study. *Geology*, *30*(1), 27–30. https://doi.org/10.1130/0091-7613(2002)030<0027:LEOTBM>2.0.CO;2.

Currie, C. A. (2016). The Deep Roots of the Rocky Mountains: Geophysical Studies of Western Canada. *Journal of Student Science and Technology*, *9*(1). https://doi.org/10.13034/jsst.v9i1.142.

Dahlen, F. A. (1990). Critical Taper Model of Fold-And-Thrust Belts and Accretionary Wedges. *Annual Review of Earth and Planetary Sciences*, *18*(1), 55–99. https://doi.org/10.1146/annurev.ea.18.050190.000415.

Das, T., & Nolet, G. (1998). Crustal thickness map of the western United States by partitioned waveform inversion. *Journal of Geophysical Research: Solid Earth*, *103*(B12), 30021–30038. https://doi.org/10.1029/98JB01119.

DeCelles, P. G. (2004). Late Jurassic to Eocene evolution of the Cordilleran thrust belt and foreland basin system, western U.S.A. *American Journal of Science*, *304*(2), 105–168. https://doi.org/10.2475/ajs.304.2.105.

Dickinson, W., Klute, M., Hayes, M., Janecke, S., Lundin, E., McKittrick, M., & Olivares, M. (1988). Paleogeographic and paleotectonic setting of Laramide sedimentary basins in the central Rocky Mountain region. *Geological Society of America Bulletin - GEOL SOC AMER BULL*, *100*. https://doi.org/10.1130/0016-7606(1988)100<1023:PAPSOL>2.3.CO;2.

Ellis, M. (1988). Lithospheric Strength in Compression: Initiation of Subduction, Flake Tectonics, Foreland Migration of Thrusting, and an Origin of Displaced Terranes. *The Journal of Geology*, *96*(1), 91–100. https://doi.org/10.1086/629195.

Erdős, Z., Huismans, R. S., & van der Beek, P. (2015). First-order control of syntectonic sedimentation on crustal-scale structure of mountain belts. *Journal of Geophysical Research: Solid Earth*, *120*(7), 5362–5377. https://doi.org/10.1002/2014JB011785.

Erslev, E. A. (2013). 2D Laramide Geometries and Kinematics of the Rocky Mountains, Western U.S.A. In *The Rocky Mountain Region: An Evolving Lithosphere* (pp. 7–20). American Geophysical Union (AGU). https://doi.org/10.1029/154GM02.

Flowers, R. M., Wernicke, B., & Farley, K. (2008). Unroofing, incision, and uplift history of the southwestern Colorado Plateau from apatite (U-Th)/He thermochronometry. *Geological Society of America Bulletin*, *120*. https://doi.org/10.1130/B26231.1.

Gao, X., & Wang, K. (2014). Strength of stick-slip and creeping subduction megathrusts from heat flow observations. *Science*, *345*(6200), 1038–1041. https://doi.org/10.1126/science.1255487.

Giambiagi, L., Mescua, J., Bechis, F., Martínez, A., & Folguera, A. (2011). Pre-Andean deformation of the Precordillera southern sector, southern Central Andes. *Geosphere*, *7*(1), 219–239. https://doi.org/10.1130/GES00572.1.

Gleason, G. C., & Tullis, J. (1995). A flow law for dislocation creep of quartz aggregates determined with the molten salt cell. *Tectonophysics*, *247*(1), 1–23. https://doi.org/10.1016/0040-1951(95)00011-B.

Hassani, R., Jongmans, D., & Chéry, J. (1997). Study of plate deformation and stress in subduction processes using two-dimensional numerical models. *Journal of Geophysical Research: Solid Earth*, *102*(B8), 17951–17965. https://doi.org/10.1029/97JB01354.

Hirth, G., & Kohlstedt, D. (2003). Rheology of the upper mantle and the mantle wedge: A view from the experimentalists. *Washington DC American Geophysical Union Geophysical Monograph Series*, *138*, 83–105. https://doi.org/10.1029/138GM06.

Holt, W. E., & Wallace, T. C. (1990). Crustal thickness and upper mantle velocities in the Tibetan Plateau Region from the inversion of regional Pnl waveforms: Evidence for a thick upper mantle lid beneath southern Tibet. *Journal of Geophysical Research: Solid Earth*, *95*(B8), 12499–12525. https://doi.org/10.1029/JB095iB08p12499.

Humphreys, E. (2009). Relation of flat subduction to magmatism and deformation in the western United States. *Geological Society of America Memoirs*, *204*(0), 85–98. https://doi.org/10.1130/2009.1204(04).

Humphreys, E., Hessler, E., Dueker, K., Farmer, G. L., Erslev, E., & Atwater, T. (2003). How Laramide-Age Hydration of North American Lithosphere by the Farallon Slab Controlled Subsequent Activity in the Western United States. *International Geology Review*, *45*(7), 575–595. https://doi.org/10.2747/0020-6814.45.7.575.

Ibarra, F., Liu, S., Meeßen, C., Prezzi, C. B., Bott, J., Scheck-Wenderoth, M., et al. (2019). 3D data-derived lithospheric structure of the Central Andes and its implications for deformation: Insights from gravity and geodynamic modelling. *Tectonophysics*, *766*, 453–468. https://doi.org/10.1016/j.tecto.2019.06.025.

Jammes, S., & Huismans, R. S. (2012). Structural styles of mountain building: Controls of lithospheric rheologic stratification and extensional inheritance. *Journal of Geophysical Research: Solid Earth*, *117*(B10). https://doi.org/10.1029/2012JB009376.

Jordan, T. E., & Allmendinger, R. W. (1986). The Sierras Pampeanas of Argentina; a modern analogue of Rocky Mountain foreland deformation. *American Journal of Science*, *286*(10), 737–764. https://doi.org/10.2475/ajs.286.10.737.

Jordan, T. E., Isacks, B. L., Allmendinger, R. W., Brewer, J. A., Ramos, V. A., & Ando, C. J. (1983). Andean tectonics related to geometry of subducted Nazca plate. *GSA Bulletin*, *94*(3), 341–361. https://doi.org/10.1130/0016-7606(1983)94<341:ATRTGO>2.0.CO;2.

Kaus, B. J. P., Mühlhaus, H., & May, D. A. (2010). A stabilization algorithm for geodynamic numerical simulations with a free surface. *Physics of the Earth and Planetary Interiors*, *181*(1–2), 12–20. https://doi.org/10.1016/j.pepi.2010.04.007.

Kaus, B. J. P., Popov, A. A., Baumann, T. S., Pusok, A. E., Bauville, A., Fernandez, N., & Collignon, M. (2016). Forward and inverse modelling of lithospheric deformation on geological timescales. *NIC Symposium 2016 - Proceedings*, *48*, 299–307.

Kay, R. W., & Kay, S. M. (1993). Delamination and delamination magmatism. *Tectonophysics*, *219*(1), 177–189. https://doi.org/10.1016/0040-1951(93)90295-U.

Kay, S. M., & Coira, B. L. (2009). Shallowing and steepening subduction zones, continental lithospheric loss, magmatism, and crustal flow under the Central Andean Altiplano-Puna Plateau. *Geological Society of America Memoirs*, *204*, 229–259. https://doi.org/10.1130/2009.1204(11).

Kley, J., Monaldi, C. R., & Salfity, J. A. (1999). Along-strike segmentation of the Andean foreland: causes and consequences. *Tectonophysics*, *301*(1–2), 75–94. https://doi.org/10.1016/S0040-1951(98)90223-2.

Kohlstedt, D. L., Evans, B., & Mackwell, S. J. (1995). Strength of the lithosphere: Constraints imposed by laboratory experiments. *Journal of Geophysical Research: Solid Earth*, *100*(B9), 17587–17602. https://doi.org/10.1029/95JB01460.

Kusznir, N. J., & Park, R. G. (1986). Continental lithosphere strength: the critical role of lower crustal deformation. *Geological Society, London, Special Publications*, *24*(1), 79–93. https://doi.org/10.1144/GSL.SP.1986.024.01.09.

Lacombe, O., & Mouthereau, F. (2002). Basement-involved shortening and deep detachment tectonics in forelands of orogens: Insights from recent collision belts (Taiwan, Western Alps, Pyrenees). *Tectonics*, *21*(4), 12–1. https://doi.org/10.1029/2001TC901018.

Lacombe, O., & Bellahsen, N. (2016). Thick-skinned tectonics and basement-involved fold–thrust belts: insights from selected Cenozoic orogens. *Geological Magazine*, *153*(5–6), 763–810. https://doi.org/10.1017/S0016756816000078.

Laske, G., Masters, T. G., Ma, Z., & Pasyanos, M. E. (2013). Update on CRUST1.0: A 1-degree Global Model of Earth's Crust.

Li A. Z., Lee C. A., Peslier A. H., Lenardic A., & Mackwell S. J. (2008). Water contents in mantle xenoliths from the Colorado Plateau and vicinity: Implications for the mantle rheology and hydration-induced thinning of continental lithosphere. *Journal of Geophysical Research: Solid Earth*, *113*(B9). https://doi.org/10.1029/2007JB005540.

Liu, S., & Currie, C. A. (2016). Farallon plate dynamics prior to the Laramide orogeny: Numerical models of flat subduction. *Tectonophysics*, *666*, 33–47. https://doi.org/10.1016/j.tecto.2015.10.010.

Mackwell, S. J., Zimmerman, M. E., & Kohlstedt, D. L. (1998). High-temperature deformation of dry diabase with application to tectonics on Venus. *Journal of Geophysical Research: Solid Earth*, *103*(B1), 975–984. https://doi.org/10.1029/97JB02671.

Marshak, S., Karlstrom, K., & Timmons, J. M. (2000). Inversion of Proterozoic extensional faults: An explanation for the pattern of Laramide and Ancestral Rockies intracratonic deformation, United States. *Geology*, *28*(8), 735–738. https://doi.org/10.1130/0091-7613(2000)28<735:IOPEFA>2.0.CO;2.

Meeßen, C., Sippel, J., Scheck-Wenderoth, M., Heine, C., & Strecker, M. R. (2018). Crustal Structure of the Andean Foreland in Northern Argentina: Results From Data-Integrative Three-Dimensional Density Modeling. *Journal of Geophysical Research: Solid Earth*. https://doi.org/10.1002/2017JB014296.

Mescua, J. F., Giambiagi, L., Barrionuevo, M., Tassara, A., Mardonez, D., Mazzitelli, M., & Lossada, A. (2016). Basement composition and basin geometry controls on upper-crustal deformation in the Southern Central Andes (30–36°S). *Geological Magazine, 153*(5–6), 945–961. https://doi.org/10.1017/S0016756816000364.

Molnar, P., & Houseman, G. A. (2004). The effects of buoyant crust on the gravitational instability of thickened mantle lithosphere at zones of intracontinental convergence. *Geophysical Journal International*, *158*(3), 1134–1150. https://doi.org/10.1111/j.1365-246X.2004.02312.x.

Molnar, P., & Lyon-Caen, H. (1988). Some simple physical aspects of the support, structure, and evolution of mountain belts. In *Geological Society of America Special Papers*

(Vol. 218, pp. 179–208). Geological Society of America. https://doi.org/10.1130/SPE218-p179.

Mosar, J. (1999). Present-day and future tectonic underplating in the western Swiss Alps: reconciliation of basement/wrench-faulting and décollement folding of the Jura and Molasse basin in the Alpine foreland. *Earth and Planetary Science Letters*, *173*(3), 143–155. https://doi.org/10.1016/S0012-821X(99)00238-1.

Mouthereau, F., & Lacombe, O. (2006). Inversion of the Paleogene Chinese continental margin and thick-skinned deformation in the Western Foreland of Taiwan. *Journal of Structural Geology*, *28*(11), 1977–1993. https://doi.org/10.1016/j.jsg.2006.08.007.

Mouthereau, F., Lacombe, O., & Meyer, B. (2006). The Zagros folded belt (Fars, Iran): constraints from topography and critical wedge modelling. *Geophysical Journal International*, *165*(1), 336–356. https://doi.org/10.1111/j.1365-246X.2006.02855.x.

Mouthereau, F., Tensi, J., Bellahsen, N., Lacombe, O., De Boisgrollier, T., & Kargar, S. (2007). Tertiary sequence of deformation in a thin-skinned/thick-skinned collision belt: The Zagros Folded Belt (Fars, Iran). *Tectonics*, *26*(5). https://doi.org/10.1029/2007TC002098.

Mouthereau, F., Lacombe, O., & Vergés, J. (2012). Building the Zagros collisional orogen: Timing, strain distribution and the dynamics of Arabia/Eurasia plate convergence. *Tectonophysics, 532–535*, 27–60. https://doi.org/10.1016/j.tecto.2012.01.022.

Nilfouroushan, F., Pysklywec, R., Cruden, A., & Koyi, H. (2013). Thermal-mechanical modeling of salt-based mountain belts with pre-existing basement faults: Application to the Zagros fold and thrust belt, southwest Iran. *Tectonics*, *32*(5), 1212–1226. https://doi.org/10.1002/tect.20075.

O’Driscoll, L. J., Humphreys, E. D., & Saucier, F. (2009). Subduction adjacent to deep continental roots: Enhanced negative pressure in the mantle wedge, mountain building and continental motion. *Earth and Planetary Science Letters*, *280*(1), 61–70. https://doi.org/10.1016/j.epsl.2009.01.020.

Oncken, O., Chong, G., Franz, G., Giese, P., Götze, H.-J., Ramos, V. A., et al. (2006). The Andes: Active Subduction Orogeny. Springer Science & Business Media.

Pearson, D. M., Kapp, P., DeCelles, P. G., Reiners, P. W., Gehrels, G. E., Ducea, M. N., & Pullen, A. (2013). Influence of pre-Andean crustal structure on Cenozoic thrust belt kinematics and shortening magnitude: Northwestern Argentina. *Geosphere*, *9*(6), 1766–1782. https://doi.org/10.1130/GES00923.1.

Perarnau, M., Gilbert, H., Alvarado, P., Martino, R., & Anderson, M. (2012). Crustal structure of the Eastern Sierras Pampeanas of Argentina using high frequency local receiver functions. *Tectonophysics*, *580*, 208–217. https://doi.org/10.1016/j.tecto.2012.09.021.

Pfiffner, O. A. (2016). Basement-involved thin-skinned and thick-skinned tectonics in the Alps. *Geological Magazine*, *153*(5–6), 1085–1109. https://doi.org/10.1017/S0016756815001090.

Pfiffner, O. A. (2017). Thick-Skinned and Thin-Skinned Tectonics: A Global Perspective. *Geosciences*, *7*(3), 71. https://doi.org/10.3390/geosciences7030071.

Poudjom Djomani, Y. H., O'Reilly, S. Y., Griffin, W. L., & Morgan, P. (2001). The density structure of subcontinental lithosphere through time. *Earth and Planetary Science Letters*, *184*(3), 605–621. https://doi.org/10.1016/S0012-821X(00)00362-9.

Price, R. A. (1981). The Cordilleran foreland thrust and fold belt in the southern Canadian Rocky Mountains. *Geological Society, London, Special Publications*, *9*(1), 427–448. https://doi.org/10.1144/GSL.SP.1981.009.01.39.

Pysklywec, R. N., & Beaumont, C. (2004). Intraplate tectonics: feedback between radioactive thermal weakening and crustal deformation driven by mantle lithosphere instabilities. *Earth and Planetary Science Letters*, *221*(1), 275–292. https://doi.org/10.1016/S0012-821X(04)00098-6.

Ramos, V. A., & Folguera, A. (2009). Andean flat-slab subduction through time. *Geological Society, London, Special Publications*, *327*(1), 31–54. https://doi.org/10.1144/SP327.3.

Ramos, V. A., Zapata, T., Cristallini, E., & Introcaso, A. (2004). The Andean Thrust System Latitudinal Variations in Structural Styles and Orogenic Shortening, 30–50.

Saleeby, J. (2003). Segmentation of the Laramide Slab—evidence from the southern Sierra Nevada region. *GSA Bulletin*, *115*(6), 655–668. https://doi.org/10.1130/0016-7606(2003)115<0655:SOTLSF>2.0.CO;2.

Siame, L., Bellier, O., & Sébrier, M. (2006). Active tectonics in the Argentine Precordillera and Western Sierras Pampeanas. *Revista de La Asociacion Geologica Argentina*, *61*, 604–619.

Smith, D., & Griffin, W. L. (2005). Garnetite Xenoliths and Mantle–Water Interactions Below the Colorado Plateau, Southwestern United States. *Journal of Petrology*, *46*(9), 1901–1924. https://doi.org/10.1093/petrology/egi042.

Sobolev, S. V., & Babeyko, A. Y. (2005). What drives orogeny in the Andes? *Geology*, *33*(8), 617–620. https://doi.org/10.1130/G21557AR.1.

Sobolev, S. V., Babeyko, A. Y., Koulakov, I., & Oncken, O. (2006). Mechanism of the Andean Orogeny: Insight from Numerical Modeling. In O. Oncken, G. Chong, G. Franz, P. Giese, H.-J. Götze, V. A. Ramos, et al. (Eds.), *The Andes* (pp. 513–535). Springer Berlin Heidelberg. https://doi.org/10.1007/978-3-540-48684-8_25.

Spencer, J. E. (1996). Uplift of the Colorado Plateau due to lithosphere attenuation during Laramide low-angle subduction. *Journal of Geophysical Research: Solid Earth*, *101*(B6), 13595–13609. https://doi.org/10.1029/96JB00818.

Stockmal, G. S., Beaumont, C., Nguyen, M., & Lee, B. (2007). Mechanics of thin-skinned fold-and-thrust belts: Insights from numerical models. *Geological Society of America Special Papers*, *433*, 63–98. https://doi.org/10.1130/2007.2433(04).

Strecker, M. R., Alonso, R. N., Bookhagen, B., Carrapa, B., Hilley, G. E., Sobel, E. R., & Trauth, M. H. (2007). Tectonics and Climate of the Southern Central Andes. *Annual Review of Earth and Planetary Sciences*, *35*(1), 747–787. https://doi.org/10.1146/annurev.earth.35.031306.140158.

Tassara, A., Götze, H.-J., Schmidt, S., & Hackney, R. (2006). Three-dimensional density model of the Nazca plate and the Andean continental margin. *Journal of Geophysical Research: Solid Earth*, *111*(B9). https://doi.org/10.1029/2005JB003976.

Tesauro, M., Kaban, M. K., & Cloetingh, S. A. P. L. (2013). Global model for the lithospheric strength and effective elastic thickness. *Tectonophysics*, *602*, 78–86. https://doi.org/10.1016/j.tecto.2013.01.006.

Whitman, D., Isacks, B. L., & Kay, S. M. (1996). Lithospheric structure and along-strike segmentation of the Central Andean Plateau: seismic Q, magmatism, flexure, topography and tectonics. *Tectonophysics*, *259*(1–3), 29–40. https://doi.org/10.1016/0040-1951(95)00130-1.

Yonkee, W. A., & Weil, A. B. (2015). Tectonic evolution of the Sevier and Laramide belts within the North American Cordillera orogenic system. *Earth-Science Reviews*, *150*, 531–593. https://doi.org/10.1016/j.earscirev.2015.08.001.

Yuan, X., Sobolev, S. V., & Kind, R. (2002). Moho topography in the central Andes and its geodynamic implications. *Earth and Planetary Science Letters*, *199*(3–4), 389–402. https://doi.org/10.1016/S0012-821X(02)00589-7.